Available online at www.sciencedirect.com
SCIENCE DIRECT®
Thermochimica Acta 431 (2005) 81–86
thermochimica acta
www.elsevier.com/locate/tca

Phase transition behaviors of crown-ether derivative and its sodium ion complex

Yoshikazu Nishikawa [a], Takafumi Watanabe [b], Hirohisa Yoshida [b,*], Mitsuru Ikeda [a]

[a] *ATA Co. Ltd., 922-1, Mitsugi, Tsurugashima, Saitama 350-2217, Japan*
[b] *Department of Applied Chemistry, Graduate School of Engineering, Tokyo Metropolitan University, 1-1 Minami-Ohsawa, Hachioji, Tokyo 192-0397, Japan*

Received 22 October 2004; received in revised form 20 December 2004; accepted 21 January 2005
Available online 2 March 2005

Abstract

The crown-ether derivatives containing azobenzene moieties, those were expected to form assembly resulted from π–π interaction, were synthesized as new class of amphiphilic monomer. The difference of phase transition behaviors and crystal structure between metal-free crown-ether derivative (AC) and sodium ion complex (ACNa) were investigated by DSC and XRD measurements. The difference of phase transition behaviors was observed by the difference of crystal preparation processes between crystallization from solution and cooling crystallization after melted in AC. In the case of ACNa, the cold crystallization and smectic LC phase were observed.

Keywords: Crown-ether; Azobenzene; Self-assembly; Phase transition; Structure

1. Introduction

Various methods, including the application of high mechanical force, electric field and magnetic field, are used to control the higher structure of polymers. With increasing the number of molecular linkages the freedom of molecules increase, it has become more difficult to control the higher structure of polymer. The several trials are proposed to obtain the structure control polymers by controlling the structure of monomer coagulations. Although amphiphilic monomers are polymerized in the bilayer vesicles, the order structure of bilayer is vanished by polymerization [1,2]. These problems are overcome by introducing chemical modification of monomers [3,4]; the obtained polymers have high ordered structure in the scale of micro meter. Another trials are the use of liquid crystalline media as a polymerization field [5,6], which is success to control the orientation of polymers.

We have proposed the "self-assemble polymerization" to fix the high order structure of self-assemble monomer to polymer [7]. Self-assemble molecules consisted of hydrophilic, hydrophobic and polymerized parts were used for "self-assemble polymerization", and the obtained polymer showed the anisotropic structure consisting of stacked bilayers [8]. The self-assemble polymerization is available not only for amphiphilic molecules but also for self-assemble molecules containing mesogenic groups. In this study, new type of self-assemble molecules containing crown-ether and azobenzene moieties as mesogen were synthesized and the phase transitions of new molecules were investigated by DSC and the simultaneous DSC-Fourier transform infrared spectroscopy (DSC-FTIR).

2. Experimental

2.1. Materials and syntheses

The highest-grade commercially available reagents were used for syntheses of the new compounds. Purification of reaction solvents was performed using suitable method. All organic solvents were freshly distilled prior

* Corresponding author. Tel.: +81 426 77 2844; fax: +81 426 77 2821.
E-mail address: yoshida-hirohisa@c.metro-u.ac.jp (H. Yoshida).

0040-6031/$ – see front matter © 2005 Elsevier B.V. All rights reserved.
doi:10.1016/j.tca.2005.01.046

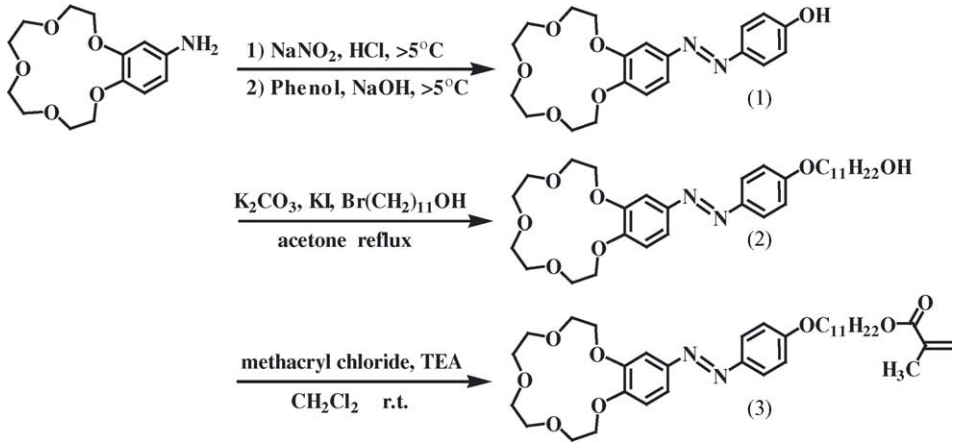

Scheme 1. Schematic diagrams of AC syntheses.

to use. Schematic diagram of syntheses route is shown in Scheme 1.

*2.1.1. Preparation of 4-[(2,3,5,6,8,9,11,12-octahydro-1,4,7,10,13-benzopentaoxacyclopentadecin-15-yl)azo]-phenol (**1**)*

An amount of 1.0 g (3.53 mmol) of 4′-aminobenzo-15-crown-5-ether and 505.8 mg (7.33 mmol) of sodium nitrite were solved in 2 ml of ice cooled 12N HCl aqueous solution. The solution was stirred for 30 min at 0 ○C. An amount of 668.2 mg (7.11 mmol) of phenol was solved in 4 M NaOH aqueous solution, was cautiously dropped into HCl solution below 5 ○C, and was stirred for 1 h. Then the reaction mixture was acidified with acetic acid. Orange precipitate was filtered and dissolved in 50 ml of chloroform and transferred to an extraction funnel. This solution was washed three times with 50 ml portions of water. The organic layer was dried over anhydrous sodium sulfate. The mixture was filtered and the solid was washed with 100 ml of chloroform. The combined solutions were evaporated and the obtained residue was purified by short silica gel column chromatograph with chloroform as the eluent to yield 4-[(2,3,5,6,8,9,11,12-octahydro-1,4,7,10,13-benzopentaoxacyclopentadecin-15-yl)azo]-phenol (**1**) as an orange solid. This solid was recrystallized twice from methanol, yielding 1.16 g (94.6%) of orange crystals. ^{1}H NMR ($CDCl_3$, TMS, δ, ppm) 3.79(s, 2H), 3.93(s, 2H), 4.21(s, 2H), 6.15(s, 1H), 6.84(m, 1H), 7.39(d, 1H), 7.52(d, 1H), 7.71(d, 2H).

*2.1.2. Preparation of 11-[4-(2,3,5,6,8,9,11,12-octahydro-1,4,7,10,13-benzopentaoxacyclopentadecin-15-ylazo)-phenoxy]-undecan-1-ol (**2**)*

To a stirred solution of 376 mg (0.969 mmol) of **1** and 277 mg (0.921 mmol) of 11-bromoundecanol, 316 mg (2.29 mmol) of potassium carbonate in 10 ml of dry acetone was placed in a 50 ml round-bottomed flask, was heated at 70 °C for 60 h under nitrogen atmosphere. Then the reaction mixture was cooled to room temperature and poured into 50 ml of ice-cooled water. Precipitate was filtered and dried under reduced pressure. The obtained residue was purified by silica gel column chromatograph with chloroform–methanol (97:3) as the eluent to yield 11-[4-(2,3,5,6,8,9,11,12-octahydro-1,4,7,10,13-benzopentaoxacyclopentadecin-15-ylazo)-phenoxy]-undecan-1-ol (**2**) as an orange solid. This solid was recrystallized from ethyl acetate, yielding 464.4 mg (85.8%) of orange crystals. ^{1}H NMR ($CDCl_3$, TMS, δ, ppm) 1.31–1.84(m, 18H), 3.62(t, 2H), 3.79(s, 8H), 3.93(s, 4H), 4.02(t, 2H), 4.21(s, 4H), 6.84(m, 1H), 7.39(d, 1H), 7.52(d, 1H), 7.71(d, 2H).

*2.1.3. Preparation of 2-methyl acrylic acid 11-[4-(6,7,9,10,12,13,15,16-octahydro-5,8,11,14,17-pentaoxa-benzocyclopentadecen-2-ylazo)-phenoxy]-undecyl ester (**3**)*

Metacryl chloride (0.12 ml, 1.24 mmol) was added to a stirred solution of 152 mg (0.273 mmol) of **2** and 0.2 ml (1.44 mmol) of triethylamine in 10 ml of dry dichloromethane. Then the solution was stirred for 24 h at room temperature under nitrogen atmosphere. After the reaction mixture was transferred to an extraction funnel. This solution was washed three times with 50 ml portions of water. Organic layer was separated and dried over anhydrous magnesium sulfate. The mixture was filtered and the solid was washed with 100 ml of dichloromethane. The combined solutions were evaporated and the obtained residue was purified by short silica gel column chromatograph with chloroform as the eluent to yield 2-methyl acrylic acid 11-[4-(6,7,9,10,12,13,15,16-octahydro-5,8,11,14,17-pentaoxa-benzocyclopentadecen-2-ylazo)-phenoxy]-undecyl ester (**3**) as a orange solid. This solid was recrystallized from ethyl acetate, yielding 100.4 mg (58.6%) of orange crystals. ^{1}H NMR ($CDCl_3$, TMS, δ, ppm) 1.31–1.94(m, 2H), 3.62(t, 21H), 3.79(s, 8H), 3.93(s, 4H), 4.02(t, 2H), 4.21(s, 4H), 5.54(s, 1H), 6.09(s, 1H), 6.84(m, 1H), 7.39(d, 1H), 7.52(d, 1H), 7.71(d, 2H).

2.1.4. Sodium ion complexation of **3**

Chloroform solution of ***3*** was vigorously stirred with saturated NaCl aqueous solution for 2 days. Organic layer was separated and solvent was removed under reduced pressure. The resulting solid was recrystallized from ethyl acetate. Identification of sodium complex of **3** was performed with FAB-MS.

2.2. DSC measurements

Differential scanning calorimetry (DSC) measurements were performed on a SEIKO Instruments Inc. DSC6200 calorimeter equipped with cooling control unit. Scanning rate was 5 K min^{-1} in a flowing nitrogen atmosphere (50 cm min^{-1}). All samples were recrystallized and completely dried under reduced pressure before measurements.

2.3. X-ray diffraction measurements

X-ray diffraction (XRD) profiles were collected using a MAC science M21XSRA X-ray diffractometer, operating in step scan mode, with Cu Kα radiation (0.154052 nm). Patterns were collected in the range 2–40° 2θ with a step size of 0.02° and a rate of 30 s per step. Samples for XRD measurements were pretreated heating to melting point and crystallization.

2.4. Simultaneous DSC-FTIR measurements [9]

The simultaneous DSC-FTIR measurements were performed on a JASCO FTIR620 equipped with the simultaneous DSC instrument [10] at 5 K min^{-1}. The detector for IR measurement was used HgCdTe (MCT) detector cooled by liquid nitrogen. Time resolution and wavelength range was used 15 s and 650–4000 cm^{-1}, respectively. Samples for simultaneous DSC-FTIR measurements were mixed 4 mg of KBr powder and about 1 mg of crown derivatives, and mixture was pressed by hand press. Prepared KBr disk was clamped in aluminum DSC vessel with a hole in the middle.

2.5. Simultaneous DSC-SAXRD measurements [11]

Simultaneous DSC-SAXRD measurements were performed by using a synchrotron radiation X-ray scattering spectrometer, equipped with the simultaneous DSC instrument, installed at the BL10C line of the 2.5 GeV storage ring in the Photon Factory of National Laboratory for High Energy Accelerator Research Organization, Tsukuba, Japan. The monochromatic synchrotron radiation X-ray using by double Si crystals was used for the simultaneous DSC-SAXRD measurement. The wavelength of X-ray was 0.1488 nm and the distance between sample and one-dimensional position sensitive proportional photon counter (PSPC) was 87 mm. Time resolution of XRD was 19 s. Under this condition, temperature resolution of one XRD profile per 2 °C was obtained. Sample for DSC-SAXRD measurement was pressed by hand press. Then the prepared sample disk was lapped with aluminum film and clamped in aluminum DSC vessel with a hole in the middle.

3. Results and discussion

DSC curves of 2-methyl-acrylic acid 11-[4-(6,7,9,10,12,13,15,16-octahydro-5,8,11,14,17-pentaoxa-benzocyclopentadecen-2-ylazo)-phenoxy]-undecyl ester (AC) are shown in Fig. 1. DSC heating curves of the solution grown crystal (SGC) (Fig. 1a) showed three endothermic transitions at 358.6 (ΔH = 37.8 kJ mol^{-1}), 377.5 (ΔH = 45.4 kJ mol^{-1}) and 383 K (ΔH = 0.65 kJ mol^{-1}). As the wide angle X-ray diffraction (WXRD) peaks disappeared at 377 K, the transition at 377 K was assigned to the melting. The transition entropies of these transitions were 105.5, 120.2 and 1.7 J K^{-1} mol^{-1}, respectively. After melting, sample was cooled at 5 K min^{-1} from the molten state. DSC cooling curve (Fig. 1c) showed one exothermic peak due to crystallization, which was confirmed by WXRD measurement. DSC heating curve of the sample obtained by cooling at 5 K min^{-1} from the molten state, melt-cooling crystal (MCC) (Fig. 1b) showed one endothermic peak due to the melting at 379.7 K (ΔH = 48.7 kJ mol^{-1}, ΔS = 128.3 J K^{-1} mol^{-1}), which was slightly higher than the melting of SGC. From the comparison of ΔH values of SGC and MCC, the melting peak of MCC was expected to include the melting and the transition at 383 K observed for SGC. DSC cooling curves of both SGC and MCC were almost the same, showed one exothermic peak at 372.5 K (ΔH = −47.8 kJ mol^{-1}), which indicated the melting and the crystallization of MCC were thermo-reversible.

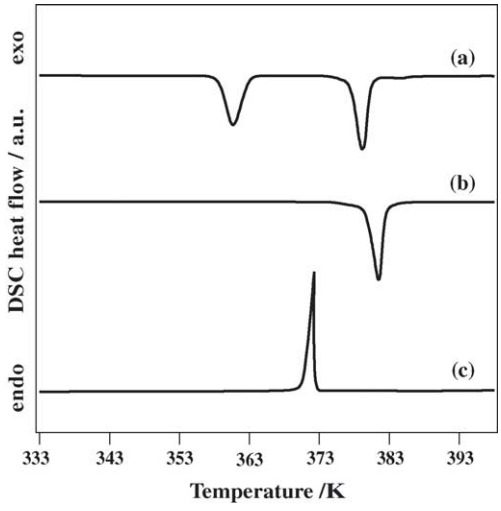

Fig. 1. DSC curves of AC, heating curve of the solution grown crystal (SGC) (a), heating curve of crystal prepared by cooling from the molten state (MCC) (b) and cooling curve from the molten state (c).

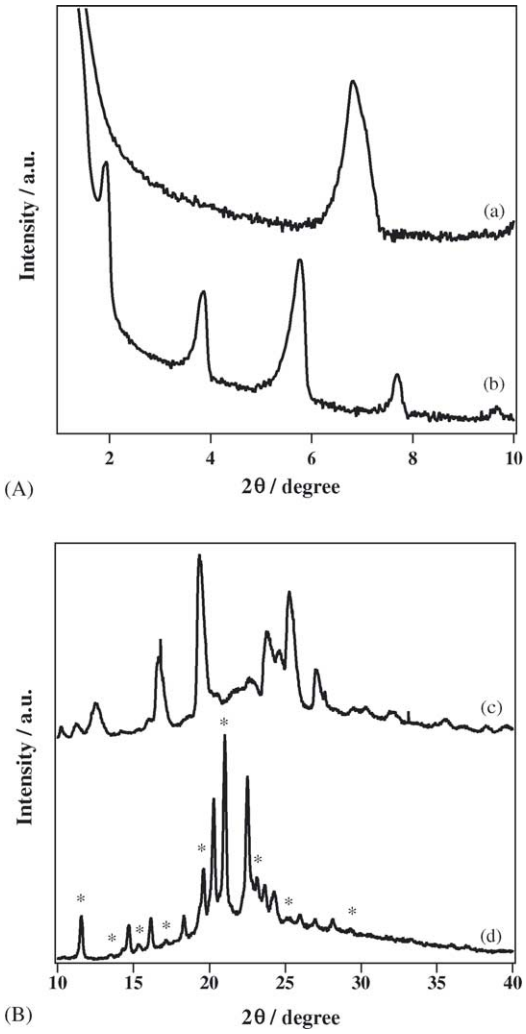

Fig. 2. XRD profiles of SGC (a, c) and MCC (b, d) of AC. The marked peaks shown in profile (d) indicate (0 0 *n*) planes.

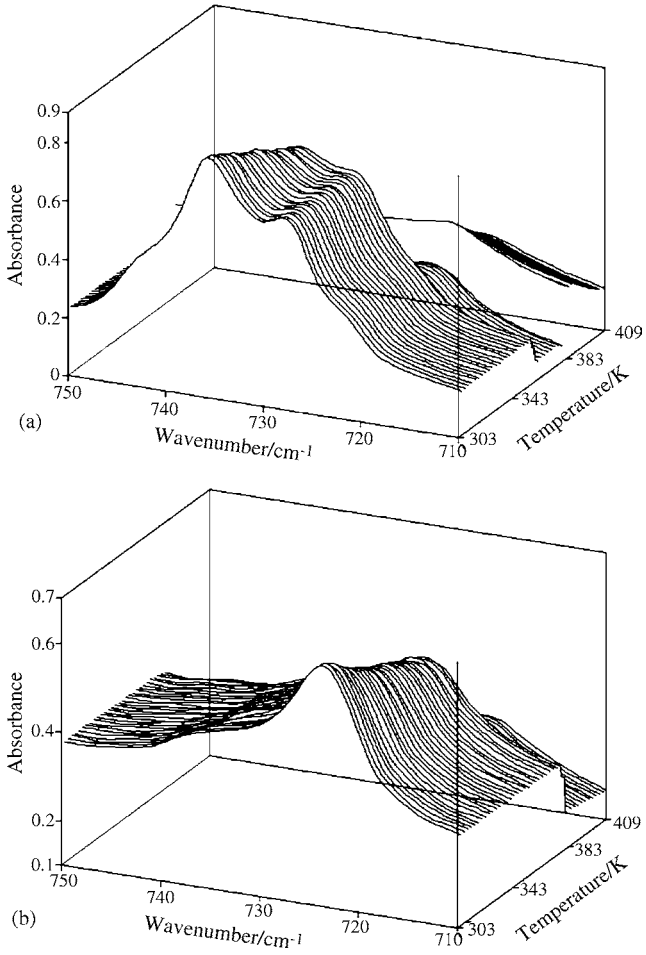

Fig. 3. Stacked FTIR spectra of SGC (a) and MCC (b) of AC observed by DSC-FTIR method on heating.

Small angle X-ray diffraction (SAXS) and WXRD profiles of SGC and MCC of AC are shown in Fig. 2. SAXS profile of MCC (Fig. 2A(b)) showed the diffraction peaks corresponding to (0 0 1) and it's high-ordered peaks (0 0 *n*) until $n = 13$ which appeared in WXRD (marked peaks in Fig. 2B(d)). These results suggested that MCC formed high ordered lamellar structure. However, XRD profiles of SGC of AC (Fig. 2(a) and (c)) differed from XRD profiles of MCC. XRD results indicated that SGC and MCC of AC were in the different crystalline forms.

The transition at 358 K was corresponding to conformational transition of alkyl chain in the crystal lattice which was identified by the simultaneous DSC-FTIR measurement. Fig. 3 shows the stacked FT-IR spectra of SGC (a) and MCC (b) obtained by heating at 5 K min^{-1}. The absorbance peaks in the wavenumber range between 720 and 740 cm^{-1} is assigned to the rocking vibration of methylene groups. The doublet peaks of CH_2 rocking vibration at 735 and 725 cm^{-1} observed for SGC indicated that the rotational motion of alkyl chains stopped completely in the crystalline state. The absorbance at 735 cm^{-1} decreased gradually with increasing temperature up to 359 K. The doublet peaks changed to the single peak at 360 K, which indicated the rotational motion of alkyl chains occurred at the transition at 358 K. The absorbance of single CH_2 rocking vibration band decreased at the melting. The doublet peaks of CH_2 rocking vibration were observed scarcely during cooling to room temperature. The single peak of CH_2 rocking vibration was observed for MCC at temperatures below 358 K. This result indicated that the rotational motion of alkyl chains allowed in the crystalline state of MCC. The transition entropy (105.5 J K^{-1} mol^{-1}) is too large to consider the rotational motion of alkyl chains as the molecular mechanism of the transition at 358.6 K, suggests that the transition at 358 K included another mechanism addition with the rotational mode of alkyl chains.

DSC curves of the two types of crystals, SGC and MCC of AC–sodium ion complex (ACNa) are shown in Fig. 4. DSC heating curve of as-prepared ACNa (SGC) shows two endothermic transitions at 353 and 363 K. The transition enthalpies of both endothermic peaks were 38 and 26 kJ mol^{-1}, which were determined by the peak separa-

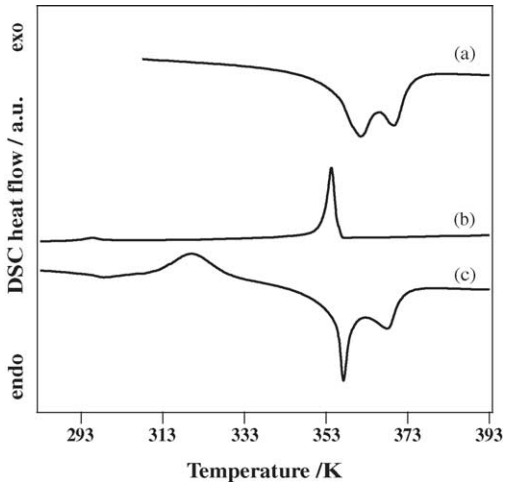

Fig. 4. DSC curves of AC-sodium ion complex (ACNa), heating curve of SGC (a), MCC (c) and cooling curve (b).

tion method. DSC cooling curve of ACNa shows a single exothermic peak at 358.6 K ($\Delta H = -32.3\,\mathrm{kJ\,mol^{-1}}$) accompanying with a small exothermic shoulder at higher temperature side. Heating DSC curve of ACNa (MCC) shows glass transition at 293 K, the cold crystallization between 310 and 325 K ($\Delta H = -19.6\,\mathrm{kJ\,mol^{-1}}$), and two endothermic transitions at 353 ($\Delta H = 34\,\mathrm{kJ\,mol^{-1}}$) and 364 K ($\Delta H = 26\,\mathrm{kJ\,mol^{-1}}$). From WXRD, the endothermic transition at 353 K of SGC and MCC of ACNa was due to the melting. XRD measurement of MCC of ACNa showed (0 0 1), (0 0 2) and (0 0 3) diffraction peaks indicating the lamellar structure. The order of the lamellar structure of MCC of ACNa was lower than that of the lamellar structure of AC.

DSC heating curve of MCC of ACNa (Fig. 4(c)) indicated that the crystallization rate of ACNa was slower than that of AC (Fig. 1). Generally the crystallization rate of molecules consisted of aryl group is faster than molecules consisted of alkyl group, because high coagulation ability due to π-electron interactions. In order to clarify the mechanism of crystallization and the transition at 364 K, the simultaneous DSC-SAXS measurement was carried out for MCC of ACNa.

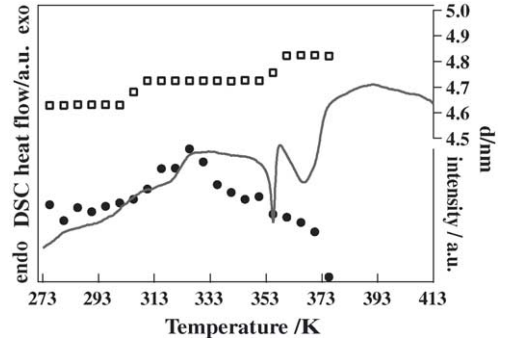

Fig. 5. Temperature changes of the lattice spacing of (0 0 1) plane (open square), of the intensity of (0 0 1) peak (solid circle) and DSC curve of ACNa obtained by DSC-XRD on heating.

Fig. 5 shows the lattice spacing of (0 0 1) plane and the intensity of (0 0 1) peak overlapped with DSC curve, which were observed during heating at $5\,\mathrm{K\,min^{-1}}$. DSC curve showed the exothermic peak due to cold crystallization between 310 and 340 K and two endothermic peaks at 353 and 364 K, these phase transitions were same to DSC result shown in Fig. 4(c). At the cold crystallization, the XRD intensity and the lattice spacing were increased. The diffraction from (0 0 1) plane remained at temperature above the melting and disappeared after the transition at 364 K. These results suggested that ACNa formed the smectic phase above the melting and the transition at 364 K was the isotropic transition. The spacing of smectic layer was expanded slightly from the lattice spacing of (0 0 1). The lamellar structure of MCC of ACNa and AC were similar to the smectic layer structure. This means that the azobenzene units acted as a mesogen of liquid crystal, and that the crystallization observed on cooling of ACNa was due to the coagulation of azobenzene units. During the cold crystallization, the increase of lattice spacing was the results of alkyl chains ordering, which disordered at the melting, because of the same transition enthalpy changes were obtained at the cold crystallization and the melting.

The cold crystallization and the smectic phase were scarcely observed for AC. ACNa has the intermolecular electrostatic repulsion interaction induced by sodium ions in crown-ether. It is considered that this repulsion force restricts the coagulation of azobenzene units, and decrease the crystallization rate of ACNa. That is to say, the repulsion force induces the smectic liquid crystalline formation.

4. Conclusions

We investigated the phase transition behaviors of AC and ACNa. In the case of AC, the SGC showed the different phase transition behaviors from the MCC. The SGC showed the solid state phase transition including the alkyl chain rotation at crystal lattice. However, the alkyl chain rotation occurred in the MCC at room temperature, which was the result of different crystal form of SGC.

In the case of ACNa, the smectic phase was observed between the melting and the isotropic transition. The crystallization rate of ACNa was slower than that of AC, the cold crystallization was observed on heating after the cooling at $5\,\mathrm{K\,min^{-1}}$ from the molten state.

References

[1] J. Leaver, A. Alonso, A. Durrani, D. Chaoman, Biochim. Biophys. Acta 732 (1983) 210–218.
[2] T. Kunitake, N. Nakashima, M. Kunitake, Macromolecules 22 (1989) 3544–3550.
[3] R. Elbert, A. Lashewsky, H. Ringsdorf, J. Am. Chem. Soc. 107 (1985) 4134–4141.

[4] S. Kato, T. Kunitake, Polym. J. 23 (1991) 135–146.
[5] K. Akagi, Kobunshi 51 (2002) 961–967.
[6] G. Piao, T. Otaka, T. Sato, K. Akagi, M. Kyotani, Mol. Cryst. Liq. Cryst. 365 (2001) 117–127.
[7] T. Yoshii, H. Yoshida, T. Kawai, IUPAC Polymer Conference on the Mission and Challenges of Polymer Science and Technology (IUPAC-PC2002), Preprints, 2002, p. 387.
[8] T. Yoshii, T. Yamada, H. Yoshida, Proceedings of the Eighth IUMRS International Conference on Advanced Materials Symposium A-2, Abstract, 2003, p. 14.
[9] H. Yoshida, J. Therm. Anal. Calorim. 55 (1999) 679–685.
[10] H. Yoshida, R. Kinoshita, Y. Teramoto, Thermochim. Acta 264 (1995) 173–183.
[11] H. Yoshida, Thermochim. Acta 267 (1995) 239–248.